Analysis of Impulsive UWB Modulation on a Real MV Test Network

Andrea M. Tonello*, Fabio Versolatto*, and Carlo Tornelli†
* DIEGM - Università di Udine - Via delle Scienze 208 - 33100 Udine - Italy
e-mail: {tonello, fabio.versolatto}@uniud.it
† RSE SpA - Via Rubattino 54 - 20143 Milano - Italy
e-mail: carlo.tornelli@rse-web.it

***Abstract*—We investigate the use of impulsive ultrawide band (I-UWB) modulation over medium voltage (MV) power line channels for low data rate communications. In particular, we consider a MV network where a channel measurement campaign has been carried out. In this paper, we firstly describe the MV test network. We study the statistics of the MV channels in terms of both root-mean-square delay spread (RMS-DS) and average channel gain (ACG). Then, we investigate the performance of I-UWB modulation with two simple receiver structures. We also consider the effect on achievable rate and bit-error-rate of the signalling bandwidth, and I-UWB modulation duty cycle.**

I. Introduction

Nowadays, the power line infrastructure is no longer seen solely as a mean for power delivery. Rather, it has proven to be useful even for high-speed communications and/or for command/control applications. In this respect, power line communications (PLC) exploit the power line infrastructure for communication purposes.

Several PLC application scenarios can be found. Indoor PLC include in-home and in-vehicle communications. Outdoor low voltage PLC focuses on the transmissions between the houses and the low voltage transformer stations, and, finally, medium and high voltage PLC consider communications beyond the low voltage transformer towards the high voltage lines. In this paper, we consider medium voltage PLC and we investigate the performance of an impulsive ultra wide band (I-UWB) modulation scheme.

Basically, impulse modulation conveys data by mapping the information symbols into short pulses. In order to cope with the channel time dispersion, pulses are followed by a guard time during which the transmitter is silent [1]. According to the FCC, impulsive modulation can be classified as ultra wide band if the fractional bandwidth, i.e., the ratio between the signalling bandwidth and the central frequency, is larger than 0.2. In PLC, since the channel attenuation strongly increases with the frequency, PLC I-UWB exploits bandwidths that are narrower than the ones of the wireless scenario [2], [3].

This work has been partly funded by the Research Fund for the Italian Electrical System under the Contract Agreement between RSE (formerly known as ERSE) and the Ministry of Economic Development - General Directorate for Nuclear Energy, Renewable Energy and Energy Efficiency stipulated on July 29, 2009 in compliance with the Decree of March 19, 2009.

The receiver is based on the matched filter concept [1]. In the presence of colored noise, the optimal implementation requires perfect knowledge of both the channel response and the noise correlation. Neglecting the noise correlation, a simpler though sub-optimal implementation of the receiver is possible.

I-UWB can be considered as an alternative to the more common orthogonal frequency division multiplexing schemes due to its simple baseband implementation and robustness against both frequency selective fading and interference. It follows that I-UWB modulation is an interesting candidate for command and control applications, where low rate reliable communications are required. In this respect, MV PLC have been recently considered for remote monitoring applications and network operational services. It should be noted that the low duty cycle of I-UWB, due to a long guard time, is such that the pulse rate is small.

The characterization of the broadband MV channel transfer function (CTF) is quite important. So far, most of the efforts have been spent on the analysis of single section MV cables [4] and only few works provide the results of measurement campaigns [5]. Furthermore, the real-world campaigns consider the low frequency range, namely up to few MHz. A bottom-up analytical model for MV networks up to hundreds of MHz has been presented in [6]. Basically, it focuses on overhead power line networks, for which it provides the MV channel response by introducing the effect of the lossy ground into the multipath propagation model [7]. The model requires a deep knowledge of the network that is typically not available in practice. Therefore, realistic broadband MV channel responses can be obtained only from measurements.

In order to investigate the performance of I-UWB modulation on real MV channels, we present the results of an experimental measurement campaign performed in the MV network that feeds the industrial complex where the RSE laboratories are located. We firstly describe the network. Then, we study the statistics of the MV channels in terms of both RMS delay spread and average channel gain. Finally, we show the performance of I-UWB modulation for the optimal and sub-optimal receiver structures and we discuss the optimal setup of the system design parameters, namely, the maximum transmit power spectral density, the bandwidth, and the guard

time duration.

The paper is organized as follows. In Section II, we describe the I-UWB system, the optimal receiver and the sub-optimal solution that neglects the noise correlation. Then, in Section III we discuss the characterization of MV channels. We both describe the test network and the main statistics of the MV channel responses. In Section IV, we show the numerical results that allow evaluating I-UWB performance on real MV channels. Finally, the conclusions are provided in Section V.

II. I-UWB System Model

We consider a binary Impulse-UWB modulation system where the information symbols are mapped into short duration pulses, namely monocycles, followed by a guard time. If the guard time is larger than the channel time dispersion, no inter-symbol interference arises and the optimal receiver is given by the matched filter receiver described in Section II-C. We assume the symbols to belong to the binary alphabet $\{-1, 1\}$ and to be transmitted with rate $1/T_f$, where T_f denotes the frame period. It follows that the transmitted signal can be written as

$$s(t) = \sum_k b(kT_f) g(t - kT_f)\,, \tag{1}$$

where $b(kT_f)$ is the transmitted symbol in the k-th frame, and $g(t)$ is monocycle used to convey the information. We shape the monocycle $g(t)$ in such a way that the transmitted signal does not occupy the lower frequencies where we experience higher levels of background noise, as it will be shown in Section II-B. We choose the conventional second derivative of the Gaussian pulse, that reads [1]

$$g(t) = \left(1 - \pi\big((t - D/2)/T_0\big)^2\right) e^{-\frac{\pi}{2}\left((t-D/2)/T_0\right)^2}\,, \tag{2}$$

where $D = 6T_0$ is the monocycle length and T_0 accounts for the duration of the main lobe. We also refer to T_g as the duration of the guard time. Hence the frame period is equal to $T_f = D + T_g$. We define the bandwidth B as the lowest frequency beyond which the frequency response of the transmitted signal is always below $30\,dB$ its maximum value. We assume the average power spectral density (PSD) of the transmitted signal to be lower than P. No form of notching is considered and thus, in the presence of coexistence constraints, the value of P has to be accurately selected. We further point out that given a PSD level, the transmitted energy is a function of the frame duration and the pulse bandwidth.

We refer to $g_{ch}(t)$ and $w(t)$ as the channel impulse response and the colored background noise, respectively. Therefore, the received signal can be written as

$$y(t) = \sum_k b(kT_f) g_{eq}(t - kT_f) + w(t)\,, \tag{3}$$

where $g_{eq}(t)$ is the equivalent impulse response of the channel, namely, $g_{eq}(t) = g * g_{ch}(t)$.

We consider a single-link packet transmission, where the packets have length 100 bits. Finally, to study the best attainable performance, we assume the channel to be perfectly known at the receiver. Practical frequency domain and simplified channel estimation algorithms have been studied in [3], [8].

A. PLC Channel

For the numerical results, the channel impulse responses $g_{ch}(t)$ have been obtained via measurements in the MV PLC network described in Section III. The acquisitions have been performed in the time domain for a maximum duration of $100\,\mu s$. Subsequently, the responses have been truncated to the ones that include 95 % of the channel energy. The measurements have validity up to 55 MHz. In Section III, more details are given about the statistics of the measured channels.

B. Noise Model

MV PLC experience high levels of background noise w.r.t. to other PLC scenarios, such as the in-home or the outdoor low voltage [9]. The MV background noise can be referred to as stationary additive Gaussian colored background noise. In particular, according to the results of the measurement campaign in [10], the noise power spectral density can be modeled as

$$N(f) = 37 \cdot e^{-0.17 \cdot f/10^6} - 105 \quad [dBm/Hz]\,. \tag{4}$$

We assume the model to be valid up to $55\,MHz$. We note that the highest levels of noise experienced in the lower frequency range fall outside the band occupied by the transmitted pulse. Therefore, the second derivative of the Gaussian pulse is suitable for the MV scenario.

C. Receiver Structures

In this paper, we focus on two types of receiver structures based on the matched filter concept [1]. In both cases, we first filter the received signal $y(t)$ with a front-end filter to obtain a decision metric. Then, we make a threshold decision on the metric to detect the transmitted bit. We refer to the front-end impulse response as $g_{fe}(t)$. Thus, the decision metric is

$$z(kT_f) = \int_{-\infty}^{\infty} y(t) g_{fe}(kT_f - t) dt\,, \tag{5}$$

where T_f is the frame duration. We further note that the decision metric $z(kT_f)$ can be written as the sum of the signal term $r(kT_f) = s * g_{ch} * g_{fe}(kT_f)$ and the noise $n(kT_f) = w * g_{fe}(kT_f)$. The k-th detected bit is then given by

$$\hat{b}(kT_f) = \mathrm{sign}\big\{z(kT_f)\big\}\,. \tag{6}$$

We always assume perfect synchronization and channel estimation. Therefore, the two receivers differ only on the front-end filter response. In the first receiver scheme, the filter is matched to the equivalent channel impulse response. We refer to this configuration as matched filter (MF) receiver. The impulse response of the MF receiver is

$$g_{fe,MF}(t) = g * g_{ch}(-t)\,. \tag{7}$$

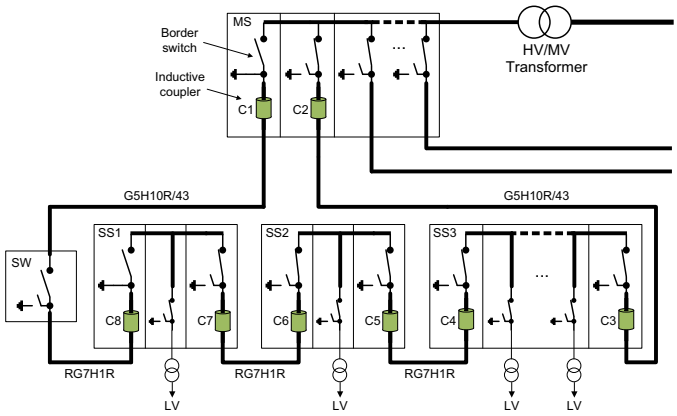

Fig. 1. Layout of the MV test network.

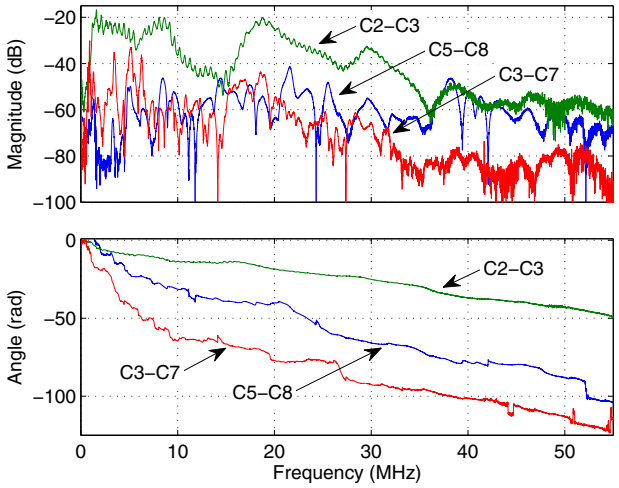

Fig. 2. Magnitude and phase of the frequency response of three different channels extracted from the MV test network.

The MF receiver has been shown to be optimal under the assumptions of stationary white background noise and no inter-symbol interference (ISI) [1]. We note that we do not experience ISI only if the guard time T_g is longer than or equal to the channel impulse response. Now, the noise in MV lines is not white and thus the MF receiver is not strictly the optimal one. The optimal receiver in the presence of colored noise is still based on the MF structure, but it takes into account for the noise correlation [1]. We refer to this receiver structure as noise-matched filter (N-MF) receiver. The impulse response of the N-MF receiver is

$$g_{fe,N-MF}(t) = R^{-1} * g_{fe,MF}(t)\,, \tag{8}$$

where $R^{-1}(t)$ is the convolutional inverse of the noise correlation function $R(t)$, i.e., $R^{-1} * R(t) = \delta(t)$.

Clearly, the N-MF receiver computes the correlation function of the noise. Therefore, it is a rather complex solution w.r.t. to the MF structure. In the following, we provide the performance of both receivers, we investigate the improvement given by the N-MF receiver, and we discuss whether it is suitable for MV power line communications.

III. Analysis of the MV Test Network

We now report the main characteristics of the MV network. We firstly describe the network in terms of interconnections and structure. Then, we provide a statistical characterization of the measured channels. We focus on the RMS delay spread and the average channel gain.

A. Network Description

We consider the MV network that feeds the industrial complex where the RSE laboratories are located. The network is representative of a scenario with a large number of users concentrated in a small area. More in detail, the network has three-phases, and it is ring shaped with four MV stations and one independent MV switch (SW), as shown in Fig. 1. The network is fed by a high voltage line via a high voltage to medium voltage (HV/MV) transformer. The HV/MV transformer is connected to a MV main station (MS) that feeds 6 MV lines. The MS is the uppermost one in Fig. 1. We refer to the other stations as substations (SS). The SS are fed by the main station via MV cable lines. In particular, since the network has a ring structure each station is connected to the two adjacent ones. The cables departing from the main station towards the substations are of type G5H10R/43, while all the other cables are of type RG7H1R.

As shown in Fig. 1, each substation contains a certain number of medium voltage to low voltage (MV/LV) transformers. In detail, there is one transformer in the substations SS1 and SS2, and 5 transformers in the substation SS3. The number of transformers is large and this emphasizes reflections and multipath effects.

Every transformer can be independently disconnected via a dedicated switch. In the same way, both ends of every MV interconnection cable terminate into a switch. We refer to these switches as border switches (BS). We feed the test network in a clockwise sense. To this aim, the switch SW and the BS towards SW are left open. All the other BS are closed. In this way, the network has a tree structure without loops.

The couplers have been placed as depicted in Fig. 1. Basically, the couplers were mounted on the end of cables inside the MV stations, and they are numbered as shown in Fig. 1. No couplers were present next to the switch SW. We used inductive couplers and we focused only on one of the three phases of the network, namely, the R-phase. Therefore, we study channels defined over a single phase.

We acquired the channel response in the time domain. Basically, we transmitted a pulse from each coupler and we collected the received pulse from all the other couplers. We did not transmit from the couplers placed on the cables towards the substation 1, namely C8 and C1. A total amount of 42 different links have been considered. As an example, in Fig. 2 we report the channel response of three links. Interestingly, we point out that the link C5-C8 lacks of electrical continuity since the border switch next to C8 is left open. This is the reason why C5-C8 exhibits a higher attenuation in the lower frequency

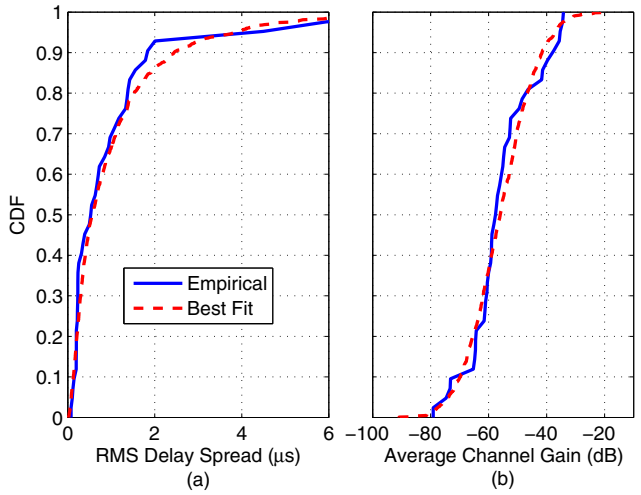

Fig. 3. On the left, CDF of the RMS-DS and its fit. On the right, CDF of the ACG in dB and its fit.

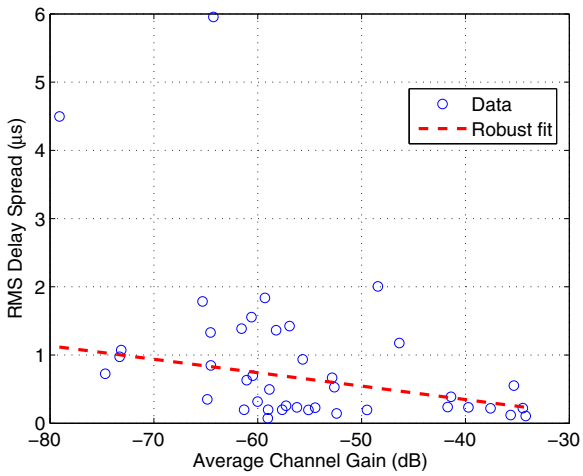

Fig. 4. RMS delay spread as a function of the ACG and its robust regression.

range, while the attenuation decreases at high frequencies, where the channel is dominated by coupling effects.

B. Statistical Characterization

Herein, we provide the statistical characterization of MV channels in terms of two important metrics, i.e., the root mean square delay spread and the average channel gain. The first metric accounts for the energy spread of the channel impulse response. Strictly, it is defined as [11]

$$\sigma_\tau = \sqrt{\frac{\sum_{i=0}^{N-1}(iT)^2|h(iT)|^2}{\sum_{i=0}^{N-1}|h(iT)|^2} - \left(\frac{\sum_{i=0}^{N-1} iT|h(iT)|^2}{\sum_{i=0}^{N-1}|h(iT)|^2}\right)^2}, \tag{9}$$

where T, $h(iT)$ and N are the sampling time resolution, the channel impulse response at instant iT and the number of impulse response points, respectively. We evaluate the RMS-DS of all the channel realizations, then we compute its cumulative distribution function (CDF). We report the result in Fig. 3a. For clarity, we limit the plot to the first $6\,\mu s$, since only one RMS-DS realization falls outside this range, i.e., $\sigma_\tau = 27.5\,\mu s$. We trace back the latter value of RMS-DS to the link C6-C3.

As already reported for other PLC scenarios [11], the RMS-DS can be considered as a lognormally distributed random variable and we have found that the best fit for the RMS-DS CDF profile is given by the lognormal distribution with mean $1.158\,\mu s$ and standard deviation $2.055\,\mu s$. In Fig. 3a, the best fit is also shown.

Now, we study the statistics of the average channel gain. The ACG is defined as follows

$$G = 10^{\frac{G_{dB}}{10}} = \frac{1}{N}\sum_{i=0}^{N-1}|H(iF)|^2\,, \tag{10}$$

where F, $H(iF)$, N and G_{dB} are the sampling frequency resolution, the channel frequency response at frequency iF, the number of frequency response points and the ACG in dB, respectively. We compute the ACG in dB for every channel realization and we provide the resultant CDF in Figure 3b and its best fit. As in other PLC scenarios [11], the normal distribution is the best fit for the CDF of the ACG in dB. The mean is $-55.56\,dB$ and standard deviation is $11.12\,dB$. Thus, the ACG is lognormally distributed.

Finally, in Fig. 4 we report the RMS delay spread as a function of the average channel gain. Again, we limit the plot to $6\,\mu s$ since only one realization falls outside this range. We have performed the robust regression analysis of the data and we have found that the slope of the robust regression line is given by

$$\sigma_{\tau,\mu} = -0.0197\,G_{dB}\,, \tag{11}$$

where $\sigma_{\tau,\mu}$ is the RMS delay spread in μs. This latter result shows that in the MV test network, for a given ACG, we experience a RMS-DS that is twice the one observed for the in-home scenario [11].

IV. Simulation Results

In this section we characterize the performance of I-UWB in the considered MV network. We simulate an I-UWB transmission over the measured channels. We study both the MF and the N-MF receivers. We present the results in terms of bit error rate (BER), achievable rate R and capacity C, with a PSD constraint. We define the achievable rate and the capacity as follows. We firstly focus on binary I-UWB with a hard decoding receiver. We model the equivalent channel as a binary symmetric channel with a probability of error equal to the BER. Therefore, we define the achievable rate as the mutual information given a statistically independent, uniform distributed binary input, i.e.,

$$R = \frac{1}{T_f}\big(1 - H(P_e)\big) \quad [bit/s]\,, \tag{12}$$

where P_e and $H(P_e)$ are the BER and the binary entropy function with probability P_e, respectively. Now, we address the

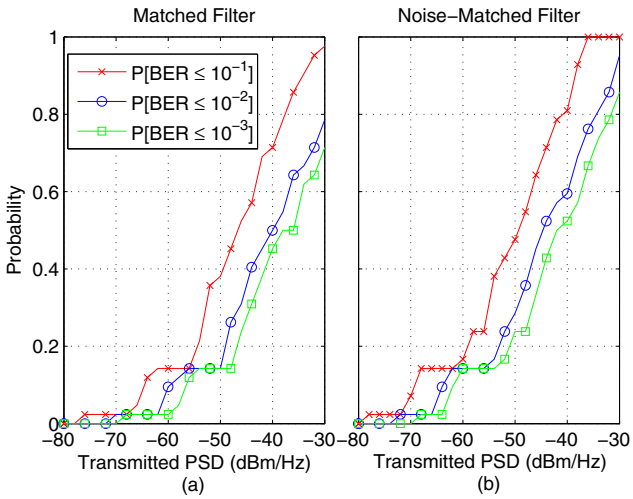

Fig. 5. CDF of the fixed BER probability for the matched filter receiver and the noise-matched filter receiver as a function of the transmitted PSD on the left and the right, respectively.

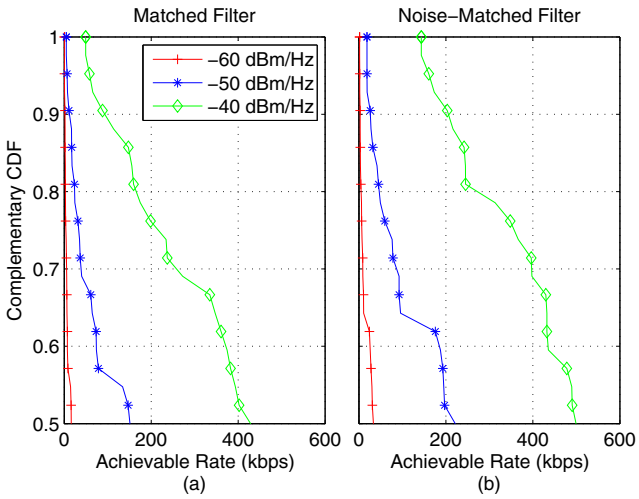

Fig. 6. Complementary CDF of the achievable rate (with hard decoding) for the matched filter receiver and noise-matched filter receiver on the left and the right, respectively. The results for three values of transmitted PSD are shown.

best attainable system performance. We let the amplitude of the transmitted signal be optimally distributed, and we assume a soft decoding receiver. According to the notation provided in Section II-C, we define the signal to noise ratio as $\gamma = \mathrm{E}[|r(kT_f)|^2]/\mathrm{E}[|n(kT_f)|^2]$, where $\mathrm{E}[\cdot]$ denotes the expectation operator. Then, the system capacity is given by

$$C = \frac{1}{T_f}\log_2\left(1+\gamma\right)\,[bit/s]\,, \tag{13}$$

since the noise is assumed Gaussian. Now, we carry out an exhaustive analysis by firstly investigating the performance of the matched filter and the noise matched filter receiver as a function of the transmitted PSD. To this aim, we vary the transmitted PSD and we let the frame duration and the pulse bandwidth assume the values of the default configuration in Table I. We note that the default configuration is not optimal a priori. In the following, we discuss the optimal set of parameters.

In Fig. 5, we provide the probability that the BER, computed over the whole set of measured channels, is less than or equal to a given value, namely, $P[BER \leq a] \quad a \in \{10^{-1}, 10^{-2}, 10^{-3}\}$. In the following, we refer to this probability as fixed BER probability. In Fig. 6 and Fig. 7, we report the complementary CDF of the achievable rate and the capacity, respectively. Clearly, the noise-matched filter receiver outperforms the matched filter receiver and it provides an average capacity increase of 1.9. Furthermore, for high values of transmitted PSD we also note that the probability that the BER is lower than 10^{-1} is 10% higher for the noise-matched filter receiver.

A. *Influence of the design parameters*

We focus on the effect of the transmitted pulse bandwidth and the frame duration. We vary each parameter individually, and we refer to the default configuration for the other values. Due to space limitations, in Fig. 8 and 9 we provide the results

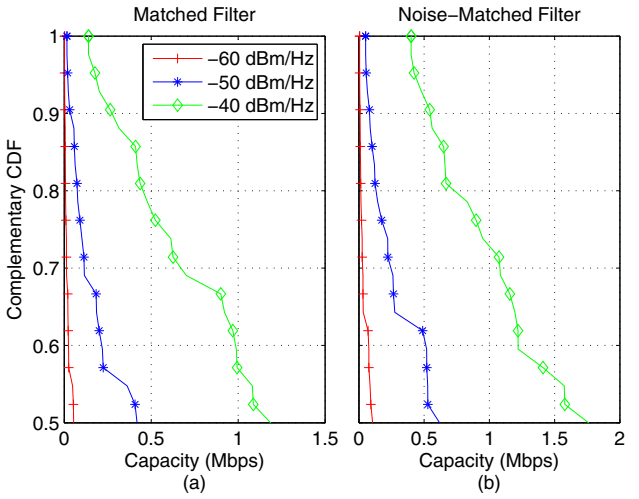

Fig. 7. Complementary CDF of the capacity for the matched filter receiver and noise-matched filter receiver on the left and the right, respectively. The results for three values of transmitted PSD are shown.

only for the optimal noise-matched filter receiver in terms of fixed BER probability and achievable rate.

From Fig. 8a, we note that the pulse bandwidth for which the probability of having a BER below a certain value is maximized, is approximately 20 MHz. Furthermore, this value leads to an achievable rate that is almost equal to 500 kbps in half of the considered channels, as shown in Fig. 8b. The

TABLE I
DEFAULT PARAMETER VALUE SET

Parameter	Value
$P\,(dBm/Hz)$	-50
$T_f\ (\mu s)$	2
$B\,(MHz)$	10

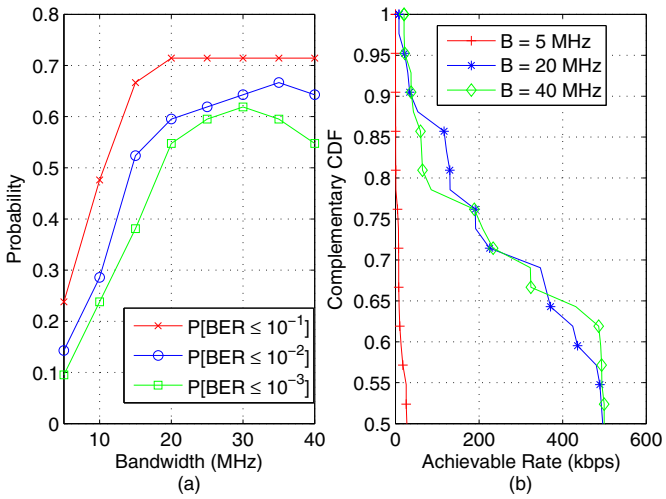

Fig. 8. CDF of the fixed BER probability and complementary CDF of the achievable rate as a function of the pulse bandwidth when the N-MF receiver is deployed on the left and the right, respectively.

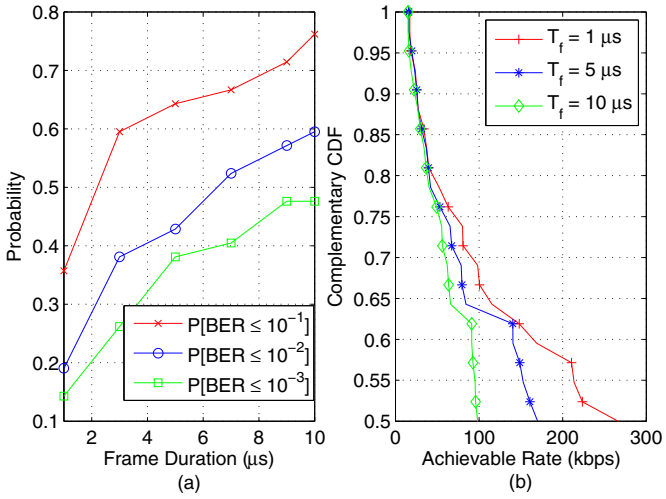

Fig. 9. CDF of the fixed BER probability and complementary CDF of the achievable rate as a function of the frame duration when the N-MF receiver is deployed on the left and the right, respectively.

drawback is given by the fact that when the pulse bandwidth increases under a PSD limit constraint, the transmitted power increases as well. Therefore, when the power consumption is a design constraint, sub-optimal solutions with narrow pulse bandwidths have to be considered. In this respect, the default configuration provides a good choice of parameters.

Now, we study the effect of the frame duration. We focus on Fig. 9b. As expected, the achievable rate decreases as the frame duration increases. For half of the channels, we have found that in the case of $T_f = 1\,\mu s$ the achievable rate is approximately 2.7 times the one obtained for $T_f = 10\,\mu s$. On the contrary, from Fig. 9a we note that the probability of having a BER lower than 10^{-2} is three times lower when $T_f = 10\,\mu s$ w.r.t. to the case of $T_f = 1\,\mu s$.

V. Conclusion

We have investigated the performance of I-UWB modulation on a real MV test network. We have described the MV network and we have addressed the statistical characterization of measured channels in terms of both RMS delay spread and average channel gain. Then, we have studied the performance of I-UWB modulation in terms of bit error rate, achievable rate of hard decoded binary I-UWB, and system capacity. We have shown the difference in performance between the optimal noise-matched filter receiver and the sub-optimal though simpler matched filter structure. We have found that the noise matched filter receiver provides an average capacity increase of 1.9 w.r.t. the matched filter receiver. Finally, we have investigated the effect of two system design parameters, namely the frame duration and the pulse bandwidth. We have found that a pulse bandwidth of $20\,MHz$ is sufficient to attain the best performance over the set of MV measured channels.

References

[1] A. M. Tonello, R. Rinaldo, and L. Scarel, "Detection Algorithms for Wide Band Impulse Modulation Based Systems over Power Line Channels," in *Proc. IEEE Int. Symp. Power Line Commun. and its App. (ISPLC)*, Apr. 2004, pp. 367–372.

[2] G. Mathisen and A. M. Tonello, "WIRENET: An Experimental System for In-House Powerline Communication," in *Proc. IEEE Int. Symp. Power Line Commun. and its App. (ISPLC)*, Mar. 2006, pp. 137–142.

[3] A. M. Tonello, "Wideband Impulse Modulation and Receiver Algorithms for Multiuser Power Line Communications," *EURASIP Journal on Advances in Signal Processing*, vol. 2007, pp. 1–14.

[4] F. Campagna, M. Quarantelli, and R. Pighi, "High-Frequency Characterization of a Medium Voltage PLC Transmission System," in *Proc. Third Workshop on Power Line Commun. and Its App. (WSPLC)*, Oct. 2009, pp. 71–73.

[5] J. J. Lee, S. J. Choi, H. M. Oh, W. T. Kee, K. H. Kim, and D. Y. Lee, "Measurements of the Communications Environment in Medium Voltage Power Distribution Lines for Wide-Band Power Line Communications," in *Proc. IEEE Int. Symp. Power Line Commun. and its App. (ISPLC)*, Apr. 2004, pp. 69–74.

[6] P. Amirshahi and M. Kavehrad, "High-Frequency Characterization of Overhead Multiconductor Power Lines for Broadband Communications," *IEEE J. Sel. Areas Commun.*, vol. 24, no. 7, pp. 1292–1303, Jul. 2006.

[7] M. Zimmermann and K. Doster, "A Multipath Model for the Powerline Channel," *IEEE Trans. Commun.*, vol. 50, no. 4, pp. 553–559, Apr. 2002.

[8] A. M. Tonello and N. Palermo, "Soft Detection with Synchronization and Channel Estimation from Hard Quantized Inputs in Impulsive UWB Power Line Communications," in *proc. IEEE Int. Conference on Impulsive Ultra-Wideband (ICUWB)*, Sep. 2009, pp. 560–564.

[9] H. C. Ferreira, L. Lampe, J. Newbury, and T. G. Swart, *Power Line Communications: Theory and Applications for Narrowband and Broadband Communications over Power Lines*. NY: Wiley & Sons, 2010.

[10] M. Babic et al., "OPERA deliverable D5. Pathloss as a function of frequency, distance and network topology for various LV and MV European powerline networks," 2005.

[11] S. Galli, "A Simplified Model for the Indoor Power Line Channel," in *Proc. IEEE Int. Symp. Power Line Commun. and its App. (ISPLC)*, Apr. 2009, pp. 13–19.